# From models to mechanisms: defects and charge trapping in amorphous silicon nitride

Hückmann, L.

**Citation**

Hückmann, L. (2026, July 2). *From models to mechanisms: defects and charge trapping in amorphous silicon nitride*. Retrieved from https://hdl.handle.net/1887/4307230

| Version: | Publisher's Version |
| --- | --- |
| License: | Licence agreement concerning inclusion of doctoral thesis in the Institutional Repository of the University of Leiden |
| Downloaded from: | https://hdl.handle.net/1887/4307230 |

**Note:** To cite this publication please use the final published version (if applicable).

# 5

# Intrinsic Charge Trapping and Reversible Charge Induced Structural Modifications in a-$Si_3N_4$



This chapter is based on

**Hückmann, L.**; Cottom, J.; Meyer, J. "Intrinsic Charge Trapping and Reversible Charge Induced Structural Modifications in a-$Si_3N_4$" *Adv. Phys. Res.* **2024**, *3*, 2300109.

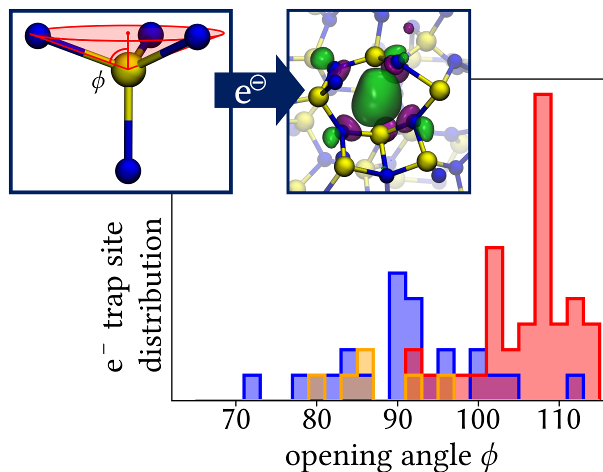

## Abstract

Amorphous silicon nitride (a-$Si_3N_4$) is an essential material for a wide variety of electronic devices, ranging from its use in dielectric layers to its paramount importance for memory applications. In particular the latter has triggered the interest in charge trapping, for which so-called N- and K-centers have been identified in experiments — with the atomistic configuration still subject of vigorous debate. Here, the range of hole and electron traps in stoichiometric a-$Si_3N_4$ are revealed by combining atomistic calculations at different levels of theory. The variety of sites within the amorphous network are characterized by introducing a statistical sampling method to quantify the statistical completeness of structural models obtained from a melt-quench procedure, in combination with a powerful local descriptor inspired by Tolman's angle. Hole trapping is dominated by 2-coordinate N-centers, resulting in shallow hole traps. In contrast, electron trapping exhibits more nuanced behavior, encompassing both intrinsic polaronic trapping and the previously identified K-center type trapping (silicon dangling bond $^*SiN_3$). Intrinsic polaronic trapping originates from distorted $SiN_4$ tetrahedra. Structural relaxation of the intrinsic polaron sites results in significant elongation of a Si-N bond and reversible generation of $^*SiN_3$ and $N_3Si–SiN_{x\in\{3,4\}}$ defects.


5

## 5.1 Introduction

Amorphous silicon nitride (a-$Si_3N_4$) is an essential material for nanoelectronics due to its excellent mechanical and electrical properties.[1] Its hardness, resistance to chemicals and irradiation, and low permeability make it widely used as a protective layer in MEMS, photovoltaics, and semiconductor chip production.[2–4] Exceptional amongst the many properties of a-$Si_3N_4$ is the ability to trap charges stably and reversibly over the long term — approximately 10 years at 150 °C.[5,6] As such, it is employed in modern non-volatile charge-trap memory devices. Generally speaking, these devices operate *via* electrons tunneling through a floating gate material by applying an electric field and getting trapped in the underlying a-$Si_3N_4$. The associated trap states are spatially localized and immobile, which allows data to be stored with good retention characteristics even when the device is turned off.[7–14]

The origin of the charge trapping and the associated memory effect in a-$Si_3N_4$ has been the subject of intense study and debate for the last 56 years since the phenomenon was first discovered.[15,16] Robertson and others identified the so-called K- and N-centers as important defect centers in a-$Si_3N_4$, with the K-center responsible for the memory effect.[17–21] Electron paramagnetic resonance (EPR) measurements provided further insights into the local environment of both the K- and N-centers. The K-centers were found to be localized on Si, with the simplest model involving a Si-dangling bond, whereas the N-center was attributed to the 2-coordinated N atoms.[21–26] Both the N- and K-centers show negative-$U$ behavior where the negative/positive charge state is favored with respect to the neutral ($2\,N^0/2\,K^0 \rightarrow N^-/K^- + N^+/K^+$).[24,27] The attribution of the N-center to undercoordinated N-sites is generally agreed upon; however, an appropriate atomistic model for the memory-active K-center is still debated. The challenge is compounded by the structural complexity inherent in amorphous and disordered thin films resulting in a wide range of potential defect environments giving rise to dramatically different trapping behaviors.



Characterizing a-$Si_3N_4$ is challenging as with all non-glass forming thin films, the amorphous phase is only stable as a strain-stabilized thin film with a significant substrate dependence on the morphology and associated properties.[28–33] This gives rise to a wide range of reported properties that depend both on the substrate and the deposition method. Reported densities vary between $\rho_a = 2.6\,\mathrm{g\,cm^{-3}}$ to $3.2\,\mathrm{g\,cm^{-3}}$ (ground state crystal reference $\beta$-$Si_3N_4$ = $3.2\,\mathrm{g\,cm^{-3}}$) with bulk modulus 150 GPa to 210 GPa ($\beta$-$Si_3N_4$ = 263 GPa). The same trends are observed in the electronic properties with a broad range of literature band gaps between 3.1 eV to 6.0 eV, with values of 4.2 eV to 5.4 eV typically reported ($\beta$-$Si_3N_4$ = 6.2 eV).[19,31,32,34–36] The combination of a broad range of properties dictated by substrate and deposition method, along with inherent averaging effects in the measurements means care must be taken in interpreting the a-$Si_3N_4$ structures.

To understand the structural complexities inherent in a-$Si_3N_4$, modeling studies have played a vital role since the earliest days. The structural models are typically produced using either classical or *ab initio* molecular dynamics *via* a melt-quench procedure.[37–41] This approach was conceived to mimic the formation of glass-forming materials (typically $SiO_2$) and while not strictly a mimic of formation for a-$Si_3N_4$, the structures produced match well with the available experimental data.[28–30] Both approaches, classical and *ab initio*, produce

comparable structures for stoichiometric a-$Si_3N_4$. When introducing defects into the melt or considering sub-stoichiometry, *ab initio* approaches are more common as they can be used without the need for reparametrizing a potential. The trade-off for this general applicability is computational time and limited supercell size.[37,39,41–44] However, it is important to note both approaches have been successfully deployed in all of the highlighted use cases producing results that accord well with experimentally characterized a-$Si_3N_4$.



The structural modeling has been complemented by defect studies utilizing periodic and cluster models of both the crystalline and amorphous $Si_3N_4$.[39,45–48] These studies have been motivated by the need to gain a more complete understanding of the charge trapping in a-$Si_3N_4$. The ultimate objective is an unambiguously agreed-upon atomistic model of the centers responsible for the memory effect. Through a combination of theory and experiment, two main candidates have emerged as the charge trapping memory (CTM) active center. With trapping either at a Si-dangling bond (most commonly referred to as the K-center) or on a Si–Si bond. These form a single defect in the crystal calculations as both motifs are found in the nitrogen vacancy ($V_N$). The calculated trapping levels show good agreement with the experimental trap levels in the band gap of $\approx \pm 1.4$ eV[49,50] above valance and below the conduction band edges, respectively.[38–40,46,50–52]

The assignment is further bolstered by experimental studies that show enhanced trapping in Si-rich regions of a-$Si_3N_4$.[51,53] It is important to acknowledge that while disagreements may persist on the exact nature of the CTM active trap, two closely related candidate defects have been identified. Indeed, the Si-Si defect at large Si-Si distances can be viewed as two Si dangling bonds as the correlation between centers decreases to zero and vice versa.

The phenomenon of intrinsic electron and hole trapping is well-known in a wide range of amorphous inorganic oxides and beyond.[54–61] In all cases, the trapping is polaronic in nature and driven by a degree of localization at the band edges as a result of varying local environments.[62] These partially localized or Anderson states[63] can lead to a dramatic increase in the polaron and bi-polaron trapping energies. As our understanding of this phenomenon has evolved, it has been found in various materials and is now known to play an important role in the leakage and breakdown of a range of amorphous oxides.[58,62] Similar polaronic trapping has yet to be identified in amorphous nitride films; however, a-$Si_3N_4$ shows a range of traps distinct from the memory active sites discussed above, with trapping

energies and concentrations similar to those identified in oxides.[17,57,64,65] How these hitherto unidentified trap states compare with the desired memory active centers and whether they contribute to the observed lateral leakage is an open question. Insights in this direction would allow the optimization of a-$Si_3N_4$ layer to both maximize the accessible trap density while reducing and ideally eliminating lateral leakage.

In this chapter, I provide new insights into charge trapping in stoichiometric a-$Si_3N_4$ and its relation to structural features at the atomic scale by combining atomistic calculations at different levels of theory. For this purpose, I introduce a statistical sampling approach for amorphous systems to quantify how a given structural descriptor converges as a function of sample size, thereby allowing an appropriate number of samples to be selected. In addition, a novel site-centered descriptor inspired by Tolman's angle is introduced to aid the analysis and characterization of the local geometry. These models are then utilized to explore the intrinsic trapping of electrons and holes in a-$Si_3N_4$. The identified trapping centers are geometrically categorized, and the link to trapping energy is demonstrated. From this analysis, a description of the trapping precursor sites is extracted and linked to the structure. Finally, the interplay between the intrinsic electron traps and the reversible and irreversible modifications to the amorphous network are described in the context of breakdown and leakage.



## 5.2 Results and Discussion

### 5.2.1 Model Validation and Characterization of Basic Properties

Before the modes of charge trapping in a-$Si_3N_4$ can be considered and linked to structural motifs, it is important to verify that the models accord with the existing experimental and computational data. Results presented here and in the following are based on a MQ procedure with cells containing 280 atoms and a cooling rate of $1\,\mathrm{K\,ps^{-1}}$, which has yielded a structural ensemble consisting of 300 samples optimized at the PBE level and a statistically representative subset of 100 samples at the HSE06 level. As already described in detail in Chapter 3, these settings have been carefully tested and consistently chosen. There is a good agreement between the approach employed here and previous experimental and the-

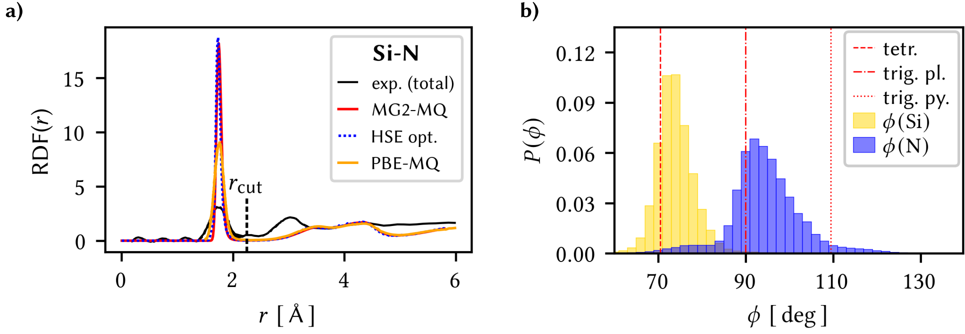


5

**Figure 5.1:** a) The radial distribution function (RDF) of silicon-nitrogen (Si–N) pairs plotted against the pair distance $r$ of the structures generated with the MG2-FF (MG2-MQ) and the optimized structures (HSE opt.). For comparison, data from a PBE-based MQ-study (PBE-MQ)[39] and X-ray diffraction experiments[28] are included. The experimental RDF cannot distinguish between elements and thus includes contributions N–N and Si–Si pairs, both of which contribute to the broad peak centered at 3.0 Å. b) Distribution $P$ of the opening angle $\phi$ for silicon (yellow) and nitrogen (blue). Red lines indicate the opening angles of the ideal tetrahedron (dashed), the ideal trigonal planar (dash-dotted), and the ideal trigonal pyramidal configuration (dotted). All data is from HSE-optimized structures.

oretical studies of a-$Si_3N_4$ (see Figure 5.1). The average a density of the a-$Si_3N_4$ models is $\rho = 2.9\,\mathrm{g\,cm^{-3}}$, which matches both experimental[16,28,29] and simulation studies.[43,66,67] Equally, the mean Si–N bond length ($r_{\mathrm{SiN}} = 1.75$ Å), mean angles ($\theta_{\mathrm{NSiN}} = 109°$, $\theta_{\mathrm{SiNSi}} = 120°$), and the mean bulk modulus ($B = 166$ GPa) agree with values reported in the literature.

The RDF for Si–N pairs in Figure 5.1a shows a sharp peak at 1.75 Å with a standard deviation of $\sigma_{\mathrm{RDF}}^{\mathrm{MG2}} = 0.04$ Å. The value agrees with the Si–N bond length in the $\beta$-$Si_3N_4$[68] and X-ray scattering experiments on a-$Si_3N_4$.[28] The shape of the curve is maintained under DFT optimization and matches the one of a fully DFT-driven MQ by Kang *et al.*[39] The local minimum after the first peak at $r_{\mathrm{cut}} = 2.25$ Å is used in the following as a short-range cut-off radius to define the first coordination sphere. It is important to note that this radius is considerably larger (28 %) than the equilibrium bond length, and the RDF does not become zero.

**Table 5.1:** Comparison in coordination number between the calculated results and the experimentally reported values[29].

| Atom type | Experiment[29] | This work (HSE) |
|---|---|---|
| Si | 3.70 | 3.96 |
| N | 2.78 | 2.87 |

Another feature of a-$Si_3N_4$ is the appearance of undercoordinated atoms; the effective coordination numbers for both elements are listed in Table 5.1. The silicon atoms are 0.37 % undercoordinated, whereas, for nitrogen atoms, the deviations are more significant, with 4.8 %. Off-coordinated atoms are a ubiquitous feature of both experimental and theoretical studies.[38–40,43] Furthermore, neutron scattering experiments by Misawa *et al.*[29] found dangling bonds are the most present defective species with coordination numbers of 3.7 and 2.78 for Si and N, respectively. However, statements on the concentration in all studies must be treated with care as an undefined portion of the signal originates from interfaces with substrates, which is not considered in these models.



An examination of the local structure in a-$Si_3N_4$ points towards considerably distorted coordination polyhedra, with a coordination sphere that is largely intact. As shown in Figure 5.1b, the distribution $P(\phi(\text{Si}))$ of the opening angles $\phi$ of the $SiN_4$ tetrahedra is shifted towards larger values than the ideal tetrahedron, with an average of $74.0^\circ \pm 3.5^\circ$ (see Chapter 3). Thus, most tetrahedra have at least one face flattened with respect to the undistorted tetrahedron. Analogously, $P(\phi(\text{N}))$ is shifted to larger values (average $94.3^\circ \pm 5.5^\circ$), indicating nitrogen being displaced out of the triangle's plane. The tails in both distributions highlight the range in coordination environments, predominantly capturing distinct sites for N and a small number of undercoordinated Si.

The examination of the electronic structure agrees with previous studies, where the valence band maximum (VBM) is predominantly N-character, and the conduction band minimum (CBM) is Si-character. A representative example of the electronic density of states (DOS) is shown in Figure 5.2. The average band-gap is 4.43 eV with localized states introduced at the band edges as confirmed in the IPR, typically assigned to the presence of coordination defects at band edges.[38–40] The localized states vary from cell to cell in number and energetic separation because the associated defective sites are not uniform in their severity of distortion. The localized states above the VBM are centered on a handful of predominantly 2-coordinated N atoms. In contrast, the ones below the CBM are centered on a distorted or 3-coordinated Si atom, which appears rarer but is associated with a higher degree of localization. It is possible that there is more than one single potential trap site per box available. Still, since the boxes get only singly charged, only the highest occupied and the lowest unoccupied state are of relevance here. The cells all have a low spin electronic ground state

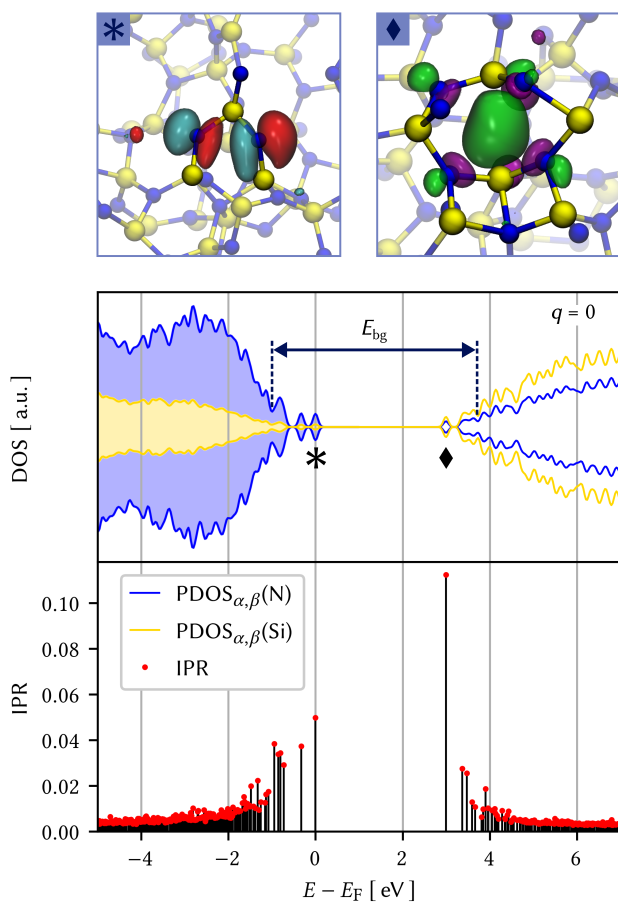


**Figure 5.2:** Upper panel: Illustration of the band edge states localized on 2-coordinated nitrogen atoms above the VBM ($*$) and localized on distorted Si-tetrahedron below the CBM (♦). The isosurfaces of the spin density are set to $0.05\,e\,\text{Å}^{-3}$. Middle panel: The projected electronic density of states (DOS) of Si (yellow) and N (blue) in a single neutral a-$Si_3N_4$ configuration relative to the Fermi level $E_F$. The band gap $E_{bg}$ is measured by excluding the localized states labeled with $*$, ♦. Lower panel: The inverse participation ratio for all eigenstates with $-5\,\text{eV} < E - E_F < 7\,\text{eV}$. All data is obtained from a DFT calculation at the HSE06 level.

such that the dangling bonds are either unoccupied or fully occupied ($N^0 + K^0 \rightarrow N^- + K^+$), in accordance with the negative-$U$ character of the dangling bond centers.[20]

### 5.2.2 Hole Trapping

As described in Section 5.2.1, the nature of the VBM is of predominately N-character, with the frontier states resulting from 2-coordinated N atoms. On the removal of an electron from the system, the hole localizes over the respective 2-coordinated N-sites making up the VBM. In the process, limited geometric relaxation takes place with an average N–Si bond elongation of 0.2 Å and the coordination sphere of all atoms remaining unaffected. This is shown schematically in Figure 5.3a. In the uncharged state, the 2-coordinated N atoms have a negative polarization compared to the 3-coordinated site. The relaxed hole state moves from the vicinity of the VBM towards the mid-gap. The average trapping energies are generally small for the majority of configurations with 0.35 eV on average as shown in Figure 5.3d. The trap levels sit in the bottom half of the band gap, with most values between the VBM



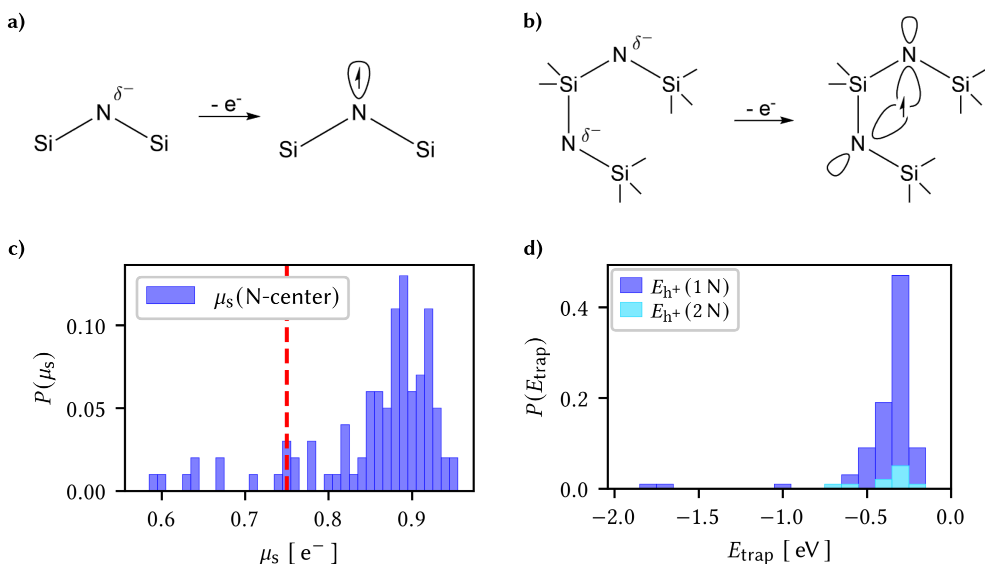


**Figure 5.3:** a) Schematic illustration of hole polaron formation by removing an electron on 2-coordinated N atom and b) on a pair of 2-coordinated N atoms. c) Distribution of spin momenta $\mu_s$ of the corresponding singly-occupied electronic state localized on N atom trapping sites. $\mu_s < 0.75\,e^-$ (red dashed line) are considered localized over two atoms. d) Distribution of hole trapping energies $E_{h^+}$ for the localized and the shared traps (1 N, 2 N).

and 1.1 eV above the VBM. This accords well with previous experimental characterization of the shallow hole traps in a-$Si_3N_4$.[69–71] Two outliers show pronounced trapping energies with trapping energies as high as −1.83 eV and result in significant relaxation.

Closer examination of the trapping sites reveals two distinct types; in most cases, the hole is localized on a single N (Figure 5.3a) with a small polarization on the neighboring N. For 10 % of the sites, the hole is shared between two adjacent 2-coordinated N (Figure 5.3b). The frequency of the 2-center trap is limited by the scarcity of 2-coordinated N and the prerequisite that two are present at adjacent sites sharing a Si center. In this case, the local environment dictates how the hole is shared between the center (Figure 5.3c). Where both centers are free to relax, the hole is evenly shared between the N atoms ($\mu_s \rightarrow 0.5$); where the relaxation of the N center is frustrated, the hole increasingly sits on a single N ($\mu_s \rightarrow 1.0$). There is no meaningful correlation in the trapping energy as a function of type, as the majority of the trapping energies sit in a narrow range with the energy range dictated by the local environment.

Altogether, these sites are analogous to the previously characterized N-centers, where the trapping energies and relaxation accord well with previous work.[21–26] The in-depth sampling presented in this thesis, adds a more nuanced perspective to the hole traps with an improved description of the electronic structure and extensive sampling of the sites available in a-$Si_3N_4$, thereby revealing the interplay between local defective structure and electronic states resulting in two different flavors of hole trapping.

### 5.2.3 Electron Trapping at K-Centers

Structurally the K-centers are similar to those previously described by Kang *et al.*[39] and others[70,72] in substoichiometric a-$Si_3N_4$. It is important to note that for stoichiometric a-$Si_3N_4$ in all cases, the ground state configuration for the 3-coordinated Si is positively charged and low spin (nominally $K^+$) as schematically depicted in Figure 5.4a. This pathway of charge trapping occurs in 31 of 100 hundred boxes within the ensemble of models. Characterization using the Tolman-inspired opening angles $\phi_K$ yields the distribution shown in Figure 5.4b, which reveals that for $q = 0$ the K-centers range from planar trigonal to the trigonal pyramidal coordination, peaked at the former, but with most structures sitting in an intermediate

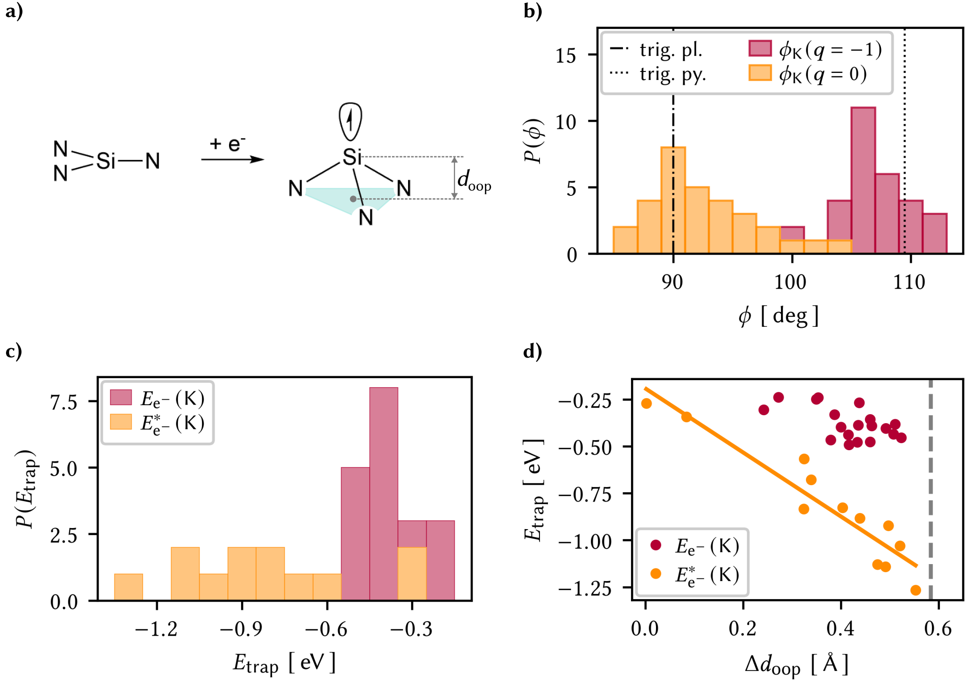


**Figure 5.4:** a) Schematic view of electron trapping at an undercoordinated Si atom with $d_{oop}$ being the distance of the silicon atom to the N–N–N plane. b) Distribution of opening angles $\phi_K$ of the trapping sites in the neutral ($q = 0$) and the charged ($q = -1$) state, with opening angles of the undistorted trigonal planar (dash-dotted line) and the trigonal pyramid (dotted line) as reference. c) Distribution of trapping energies for electrons trapped on K-centers $E_{trap}$ and d) their correlation with the change of the trigonal pyramid's height $d_{oop}$ (see a) during the trapping process. The black dashed line marks $d_{oop}$ in an ideal, undisturbed $SiN_4$ tetrahedron. The purple circles represent the data points considered for fitting the line $E^{fit}_{e^-}(\Delta d_{oop})$ and defines the group $E^*_{e^-}$, and the remainder is labeled $E_{e^-}$ (also in panel c).

geometry. On trapping an electron, the peak of this distribution changes from 92.7° to 106.7° (see $P(\phi_K(q=-1))$ in Figure 5.4b), i.e., the structure relaxes to towards trigonal pyramidal geometry and the unpaired electron occupies the vacant tetrahedral bonding site. This site emerges after the structural relaxation of the Si out of the N–N–N plane, the amount of which is quantified *via* the trigonal pyramid's height $d_{oop}$ as sketched in Figure 5.4a. The magnitude of the relaxation is typically small such that the relative distances in the first coordination shell are hardly affected. In all cases, the electron is localized on a single Si-atom leaking out slightly towards the neighboring atoms. There is a strong correlation between the position of the empty Si-state in the band gap and the geometry. In the trigonal planar configuration, the empty Si-state is degenerate with the CBM, whereas the trigonal pyra-

midal configurations give rise to mid-gap states. As a result, the majority fall between the extreme cases giving rise to states in the upper half of the band gap.

As shown in Figure 5.4c, the trapping energies are typically small with an average of −0.55 eV and the majority clustered around the mean. However, several sites show trapping energies with significantly larger absolute values as a result of the local environment. Investigating the link between the trapping energy and the magnitude of the displacement due to relaxation $\Delta d_{\mathrm{oop}}$ yields two trends visualized in Figure 5.4c and Figure 5.4d: There are some traps clustered around −0.5 eV without a meaningful link between trapping energy and displacement, with a range of displacements resulting in a narrow range of trapping energies ($E_{\mathrm{e}^-}$). In contrast, there appears to be a linear trend ($\Delta E_{\mathrm{e}^-}^{\mathrm{fit}}/\Delta d_{\mathrm{oop}} = -1.71 \pm 0.19\,\mathrm{eV\,\AA^{-1}}$) where the displacement and trapping energies are strongly correlated covering an energy range from −0.27 eV to −1.27 eV ($E_{\mathrm{e}^-}^*$) and displacements up to 0.55 Å. In both cases, the low trapping energies paired with the minor change in geometry lead to the electron being reversibly trapped.

### 5.2.4 Intrinsic Electron Trapping

The trapping considered up to this point has resulted from (under)coordination "defects" in the amorphous network providing the states that give rise to the trapping behavior. By the convention adopted in this work, electron trapping on fully coordinated atoms is considered as intrinsic trapping, which is schematically depicted in Figure 5.5a. This type of trapping occurs on initially fully coordinated Si atoms that deviate from the ideal tetrahedral symmetry (see Figure 5.5b, upper panel), analogous to intrinsic trapping in a-$SiO_2$ described in previous work.[57] Geometric relaxation is dominated by two nearest-neighbor N atoms moving away from each other by an average distance of $\Delta r_{\mathrm{intr}} = 0.2$ Å. Consequently, one face of the corresponding $SiN_4$ tetrahedron is distorted towards a pseudo trigonal bipyramid geometry whose equatorial position is occupied by the electron with local $C_{2v}$ symmetry, which is schematically depicted by the intrinsic configuration in Figure 5.5a. The average opening angle $\phi_{\mathrm{intr}}$ widens from 81° to 91° (see Figure 5.5b, lower panel, purple histogram). For 35 % (24 out of 69 simulation cells) of the intrinsic traps the relaxation stops at this point, which makes them almost iso-structural to the intrinsic electron traps described in a-$SiO_2$.[57] As shown in Figure 5.5c by the purple histogram, none of these intrinsic traps have trapping

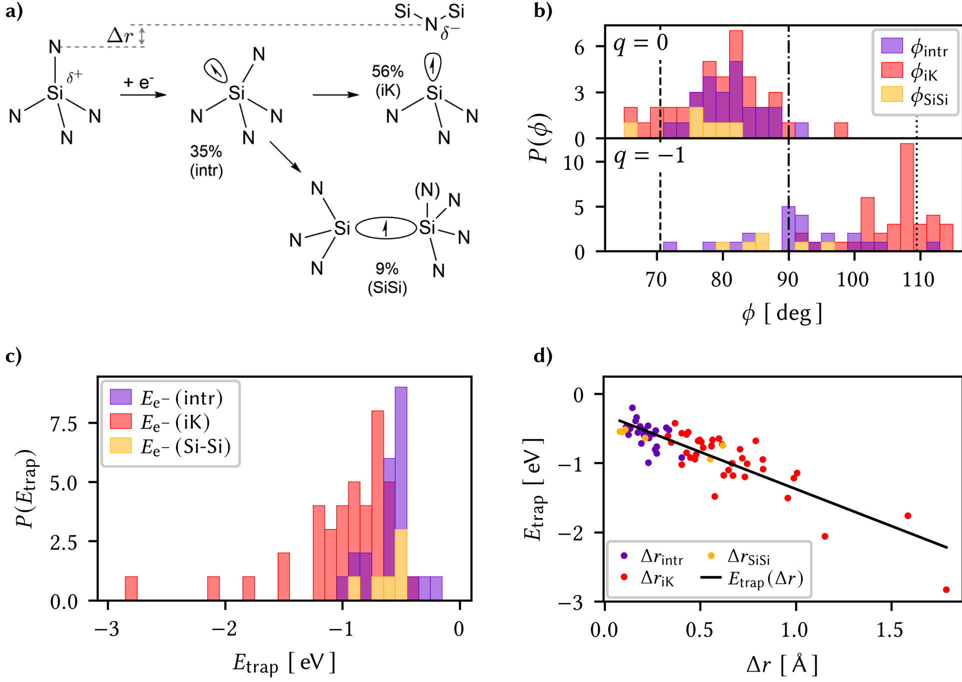


**Figure 5.5:** a) Schematic view of intrinsic electron trapping at a $SiN_4$ tetrahedron cut out of a-$Si_3N_4$, which results in intrinsic traps (intr in blue), induced K-centers (iK in red), and $N_3Si{-}SiN_{x\in\{3,4\}}$ dumbbell configurations (SiSi in yellow). b) Distribution of opening angles $\phi$ of the trap sites of these three types of trapping configurations in the neutral ($q = 0$) and charged state ($q = -1$). The opening angles of the undistorted tetrahedron (dashed line), of the trigonal plane (dash-dotted line), and of the trigonal pyramid (dotted line) are given as references. c) Distribution of the trapping energies $E_{\text{trap}}$ associated with the three types of trapping configurations. d) Correlation between $E_{\text{trap}}$ and the change of nearest Si–N neighbor distances $\Delta r$ due to geometric relaxation as schematically indicated in a).

energies less than −1.0 eV, with a distribution closely centered around its mean of −0.6 eV and only a slight skew towards smaller energies. These states show reasonable agreement with the shallow electron trap states close to the CBM of a-$Si_3N_4$.[31,73,74]

a-$Si_3N_4$ lacks the structural flexibility inherent to a-$SiO_2$ because the N anions in the former are predominantly 3-coordinated, leading to substantially frustrated geometric relaxation. In 56 % (39 out of 69 simulation cells) the relaxation of intrinsic traps continues with one of the Si–N bonds elongating significantly, resulting in the formation of a 2-coordinated N (formally $N^-$) and the unpaired electron on the emerging 3-coordinated Si ("iK" configuration in Figure 5.5a). This is iso-structural with the K-center described above as it employs

the same number of neighbors. The corresponding distribution of $\phi_{\mathrm{iK}}$ is centered at 106°, indicating the formation of a trigonal pyramid (see Figure 5.5b, lower panel, red histogram). For this reason, this subgroup of traps is referred to as induced K-centers (iK). Compared to the trapping described in Section 5.2.3 they show two important differences: Firstly, the presence of neighboring 2-coordinated N atoms, and secondly, there are no dangling bond states in the band gap prior to trapping. Both facts combined allow the vast majority of these traps to be de-trapped reversibly despite trapping energies with significantly higher absolute values and an average of −1.0 eV (see Figure 5.5c, red histogram). This does not hold for the outliers with trapping energies even below −1.5 eV. Trapping at these outlier sites results in a pronounced distortion of the amorphous network, driven by the trapping in a strained local structure. The relaxation results in the ring opening, thereby releasing strain in a given region and irreversibly altering of the amorphous network resulting in a new K-center and a 2-coordinated N atom. The third subgroup of electron trapping geometries is identified as $N_3Si{-}SiN_{x\in\{3,4\}}$ motif, which occurs in only 9 % (6 out of 69 simulation cells) and is thus the rarest one. As such, care should be taken in inferring any general behavior or trends from the ensuing characterization as a larger structural ensemble is likely required. In this case, trapping occurs on a Si–Si bond with the trapped electron shared between two Si-atoms, analogous to the N-center described for the hole trap. It is equally present in those cells that contain Si-dangling bonds and those that do not. In common with previous studies, the Si–Si trap level sits close or slightly below the CBM, although due to the limited occurrence of the $N_3Si{-}SiN_{x\in\{3,4\}}$ in the stoichiometric models presented here drawing universally valid conclusions must be done with caution. The trapping energies sit between the intrinsic electron trap and the trap-induced K-center, with an average trapping energy of −0.7 eV (see Figure 5.5c) and a wide range of Si–Si bond lengths between 2.34 Å to 2.62 Å.

All three trap types have in common that their trapping energy $E_{\mathrm{trap}}$ scales with the displacement of their nearest neighbor N atoms upon relaxation. This is illustrated in Figure 5.5d, where $E_{\mathrm{trap}}$ is plotted as a function of the largest displacement $\Delta r$ in the first coordination shell of the trap site. The linear fit to the data yields a slope of $-1.1\,\mathrm{eV\,Å^{-1}}$ with a standard deviation of $0.1\,\mathrm{eV\,Å^{-1}}$.

### 5.2.5 Discussion

As expected from the complex and nuanced view of charge trapping in a-$Si_3N_4$ presented in the literature prior to this study, a multifaceted picture of hole and electron trapping emerges from the findings in this chapter. Hole trapping in the absence of either substoichiometry or introduced defects is found to be dominated by the 2-coordinated N atoms (N-centers). The description of the N-center accords with previous studies, with trap levels close to (0.5 eV) the VBM and low trapping energies resulting in the transient nature of the trap state. The models presented here show a substantially higher N-coordination number than the experimentally characterized films.[28,29] It is therefore reasonable to conclude that undercoordinated N plays an important role in hole trapping.

5

Electron trapping initially shows two distinct modes, *i.e.,* those traps that are K-center-like, trapping on 3-coordinated Si atoms pre-existing in the network and those that are intrinsic with the trapping on fully coordinated albeit distorted Si-centers. The trapping at K-centers and $N_3Si{-}SiN_{x\in\{3,4\}}$ accords with the previous work for both the crystal[46,50,51] and the amorphous phase.[38–40] The K-center trapping levels cover a broad range of values from 0.2 eV to 2.0 eV below the CBM. The trapping energies are typically small with $E_{e^-}(\mathrm{K}) = -0.5$ eV, with a range of −0.27 eV to −1.25 eV. Finally, from the relationship between trapping energy and geometric relaxation two regimes are suggested. The first, where the trapping energy and the relaxation are decoupled, and the second where the two are strongly correlated.

The intrinsic electron traps are polaronic in nature and driven by a partial localization of the CBM as a result of distorted $SiN_4$ motifs. The trap levels show some overlap with the K-centers described in the previous paragraph, although sit in a much tighter range, close to the CBM. On the trapping of an electron the electron is fully localized on a fully coordinated Si, there is a relaxation that results in two bonds elongating and an opening of one face of the corresponding $SiN_4$ tetrahedron. Until this point the relaxation is analogous to that described for intrinsic electron polarons in $SiO_2$.[56,57,62] The relaxation is limited compared to a-$SiO_2$ as the increased nodal connectivity of the anion increases cross-linking and reduces flexibility in the network. As a result the trapping energies are lower — approximately 50 % of those of a-$SiO_2$— at an average $E_{e^-} = -0.6$ eV, with a range of −0.2 eV to −1.0 eV. The traps are reversible with respect to discharge and result in a recovery of the original geometry and energy.

All of the intrinsic electron traps initially relax as described in the previous paragraph, for 65 % of the intrinsic traps the relaxation continues giving rise to either the trap-induced K-center (56 %) or a trap-induced $N_3Si{-}SiN_{x\in\{3,4\}}$ (9 %). For the trap-induced K-center, the trapping energies are more pronounced with an average $E_{e^-}(\text{iK}) = -1.0$ eV, with a range −0.5 eV to −2.8 eV. For all but the highest trapping energies the trapping is reversible. The configurations with the highest trapping energies induce significant changes to the lattice, thereby allowing strained motifs to relax. The magnitude of the relaxation (>1 Å) makes recovery of the original structure impossible. A similar picture emerges for the trap-induced $N_3Si{-}SiN_{x\in\{3,4\}}$, the initial relaxation elongates a Si—N bond, and for the trap-induced K-center the relaxation is dominated by the N moving away. In the induced $N_3Si{-}SiN_{x\in\{3,4\}}$ the local environment both the N and Si relax resulting in the back projection of Si through the N-plane where it interacts with an adjacent distorted $SiN_4$ that undergoes relaxation to form $N_3Si{-}SiN_{x\in\{3,4\}}$. For the defects described here, the process is reversible although as previously noted the limited sampling of the induced $N_3Si{-}SiN_{x\in\{3,4\}}$ makes definitive statements impossible.

There is to note that there is no analogous single electron process seen in the intrinsic trapping behavior of a-$SiO_2$ — which is considered as reference system here. Forming an electron bi-polaron has been shown to result in an oxygen atom being pushed into an interstitial where the excess charge is being localized ($O_i^{2-}$), leaving a neutral oxygen vacancy ($V_O^{\,0}$) behind. This process either happens spontaneously or *via* a small barrier. The frustrated relaxation in a-$Si_3N_4$ favors the elongation of a Si—N bond, the same lack of flexibility ensures the reversibility of the process, trapping the 2-coordinated N in the vicinity of the 3-coordinated Si. Resulting in a modification to the amorphous network both reversibly and irreversibly upon the trapping of a single electron requires careful consideration. In a-$SiO_2$ a single electron is trapped reversibly at wide O—Si—O bond angles, whereas the electron bi-polaron results in an irreversible modification to the lattice as noted. For a-$Si_3N_4$ an intermediate behavior is found, the electron trapping begins being analogous to a-$SiO_2$ showing similar initial trapping geometries and relaxations, albeit frustrated as a result of increased anion connectivity. The lack of structural flexibility drives the structural modifications that result in trap-induced K-centers and $N_3Si{-}SiN_{x\in\{3,4\}}$. What is both interesting and perhaps unexpected is that both of the active defects in charge trapping memory are reversibly generated as a result of intrinsic electron trapping.

The trap-induced formation of K-centers has important implications for the understanding of defect concentration and how it may evolve over a series of charge/discharge cycles, *i.e.,* read/write cycles in memory device applications. It also makes the K-center concentration something of a moving target, as some K-centers will be invisible prior to charging and upon charging the defect levels sit in an identical range to the native K-centers. Lateral leakage in this context will be mediated by the trap concentration and distribution in the material, and as such intrinsic traps, induced and native K-centers would play a role. From an application perspective, the presence of the trap-induced K-center — while not the target trapping center — has the same characteristics as the native K-center. So it would not be expected to be detrimental to performance, aside from the potential role in lateral leakage previously referenced and dictated by concentration.[72,75,76] For a-$Si_3N_4$ in gate dielectric applications, the implications are potentially more serious, the propensity for intrinsic trapping and the generation of trap-induced K-centers would provide a vector for the charging of the dielectric layer. The implication being that the threshold voltage instability and time-dependent dielectric breakdown are driven *via* intrinsic trapping and as such difficult to avoid. Finally, in the case of a-$Si_3N_4$ ReRAM this sheds light on the process of electro-forming and switching in a-$Si_3N_4$, with intrinsic trapping as the first step, followed by structural relaxation to generate the conductive filament. The high resistance state is then recovered *via* the reverse process, hole-trapping followed by structural relaxation to recover the original structure.



## 5.3 Conclusion and Summary

In summary, the nuanced modes of hole and electron trapping within stoichiometric a-$Si_3N_4$ have been investigated by combining atomistic calculations at the force field and DFT level with both PBE and HSE06. By applying the statistical sampling method introduced in Chapter 3 to quantify the statistical completeness of structural models obtained from a melt-quench procedure, in combination with a powerful local descriptor inspired by Tolman's angle, both structural and energetic properties of the variety of sites within the amorphous network have been systematically characterized and correlated. Hole trapping is found to be *via* 2-coordinated N, which make up the VBM. The trapping energies are in general low and there is little perturbation to the lattice in agreement with previous observations. This sug-

gests that in stoichiometric a-$Si_3N_4$ 2-coordinated N dominate the shallow hole traps. The electron trapping shows two initial trapping modes either *via* K-centers, where the electron localizes either on a single 3-coordinated Si or on a fully coordinated Si forming an intrinsic electron polaron. For 35 % of the intrinsic trap sites the relaxation stops at this stage. However, the majority (65 %) of the intrinsic electron traps relax further forming either a trap-induced K-center (56 %) or $N_3Si{-}SiN_{x\in\{3,4\}}$ (9 %). These result in a reversible modification to the amorphous network that leads to analogs of the much-discussed defects in charge trapping memory. This intrinsic trap-induced defect formation requires a revision to our understanding of trap states in a-$Si_3N_4$, as the concentration measured is intrinsically linked to the observation conditions. Finally, this provides important insights to the mechanism of leakage in a-$Si_3N_4$ films and electro-forming in a-$Si_3N_4$ ReRAM.



## 5.4 Computational Details

A two-stage model-building approach is employed utilizing classical molecular dynamics to produce the initial amorphous structures, with subsequent revision of the MD geometries and electronic structure calculations with density functional theory (DFT). The MG2 potential[41] and the LAMMPS[77] code were selected to generate the initial models *via* a classical MD melt-quench procedure applied to periodic 280 atom cells of $\beta$-$Si_3N_4$. The MG2 potential was selected as it has previously been demonstrated to produce structural models that accord well with the experimentally characterized films.[42,43,78] A range of box sizes (112, 280, 336, 672, and 1512) and cooling rates (0.1, 1, 10 K ps$^{-1}$) were tested to ensure any size and cooling rate effects were understood and the boxes taken to production were free of such artifacts. The full results of the box size and cooling rate convergence tests are included in Chapter 3; the only point of note is a large structural instability was observed in the smallest boxes containing 112 atoms — a size that has been used for fully DFT-based simulations before.[39,67] The MQ was performed using a simulation time step of 0.5 fs. The Nosé-Hoover thermostat and barostat[79–81] were applied to control the *NpT* conditions with coupling constants set to the hundred- and thousandfold of the simulation time step. Ring statistics were performed with the RINGS software package[82] employing the primitive rings algorithm[83,84] and a cut-off of $r = 2.25$ Å. An initial ensemble size of

300 boxes was converged based upon the sampling methodology outline in Section 3.3; upon hybrid-DFT optimization the sample size was further reduced to 100 boxes.

The DFT calculations are performed spin-polarized using CP2K[85] with the DZVP-SR-MOLOPT[86] family of basis-sets to describe the valence electrons, and the GTH pseudopotentials[87,88] to describe the core electrons. An energy cutoff of 650 Ry and a relative cut off of 70 Ry was used to achieve an initial convergence of 0.1 meV per formula unit, including only the Γ-point for Brillouin zone sampling in the simulation cells containing 280 atoms. The lattice vectors and ion positions were relaxed using the quasi-Newton BFGS update scheme. The convergence criteria were $1 \times 10^{-7}$ eV and 0.005 eV $\text{Å}^{-1}$ for forces. An initial pre-optimization with the PBE[89,90] functional was performed to provide an improved initial guess for the wave function (and geometries), followed by an optimization with HSE06.[91,92] The auxiliary density matrix method (ADMM)[93] was employed for production as it significantly reduces the computational overhead for the hybrid functional calculations. In each case both the lattice vectors and ion positions are fully relaxed, ion positions only for the trapping calculations. The trapping energy is described as the energy of the localized charge carrier referenced to that of the free carrier (hole or electron) in the conduction or valence band. As a result all trapping energies are 0 bound (no charge localization) with increasingly negative trapping energies describing more energetically favored trap states. The multiplicity of the system is allowed to relax from both the low spin (all electrons are paired) and a high spin (all undercoordinated atoms have an unpaired electron) initial guess to ensure the same solution is found and the ground state multiplicity described. The reversibility of the trapping process is determined by re-optimizing the charged geometries in the neutral charge state to ensure the original structure (and energy) is recovered, and to explore those cases where trapping leads to an irreversible change to the network. To account for finite size charge effects the Lany-Zunger[94,95] correction scheme was applied. The degree of localization is gauged from the (dimensionless) inverse participation ratio

$$\mathrm{IPR}(i) = \frac{\sum_j c_{ij}^4}{\left(\sum_j c_{ij}^2\right)^2}\,, \tag{5.1}$$

where $c_{ij}$ refers to the expansion coefficients of the $i$-th Kohn-Sham state in Gaussian-type orbital part of the CP2K basis set. The same concept has been used extensively to gauge the degree of localization of electronic and vibrational states in amorphous and disordered

films,[59,96–100] *i.e.,* the higher the IPR value the stronger the localization. The band gap is then taken from the mobility edge of the valence band to the mobility edge of the conduction band, so as not to take into account the localized states that comprise the band edges.[98] Visualization and rendering were performed using the visual molecular dynamics (VMD) package.[101]



## References


[1] Meena, J. S.; Sze, S. M.; Chand, U.; Tseng, T.-Y. *Nanoscale Res. Lett.* **2014**, *9*, 526.

[2] Doo, V. Y.; Nichols, D. R.; Silvey, G. A. *J. Electrochem. Soc.* **1966**, *113*, 1279.

[3] Okada, A. *J. Eur. Ceram. Soc.* **2008**, *28*, 1097–1104.

[4] Riley, F. L. *J. Am. Ceram. Soc.* **2000**, *83*, 245–265.

[5] Lina, S. H.; Chin, A.; Yeh, F. S.; McAlister, S. P. In *2008 IEEE International Electron Devices Meeting*, IEEE: San Francisco, CA, USA, 2008.

[6] Shaposhnikov, A.; Petrov, I.; Gritsenko, V.; Kim, C. *Phys. Solid State* **2007**, *49*, 1628–1632.

[7] Arreghini, A.; Driussi, F.; Vianello, E.; Esseni, D.; van Duuren, M. J.; Golubovic, D. S.; Akil, N.; van Schaijk, R. *IEEE Trans. Electron Devices* **2008**, *55*, 1211–1219.

[8] Lu, C.-Y. *J. Nanosci. Nanotechnol.* **2012**, *12*, 7604–7618.

[9] Wang, L.; Yang, C.-H.; Wen, J. *Electron. Mater. Lett.* **2015**, *11*, 505–543.

[10] Gismatulin, A. A.; Kamaev, G. N.; Kruchinin, V. N.; Gritsenko, V. A.; Orlov, O. M.; Chin, A. *Sci. Rep.* **2021**, *11*, 2417.

[11] Chen, Y. *IEEE Trans. Electron Devices* **2020**, *67*, 1420–1433.

[12] Herrmann, M.; Schenk, A. *J. Appl. Phys.* **1995**, *77*, 4522–4540.

[13] Fujisaki, Y. *Jpn. J. Appl. Phys.* **2013**, *52*, 040001.

[14] Padovani, A.; Larcher, L.; Heh, D.; Bersuker, G.; Della Marca, V.; Pavan, P. *Appl. Phys. Lett.* **2010**, *96*, 223505.

[15] Hu, S. M.; Kerr, D. R.; Gregor, L. V. *Appl. Phys. Lett.* **1967**, *10*, 97–99.

[16] Chu, T. L.; Szedon, J.; Lee, C. *Solid-State Electron.* **1967**, *10*, 897–905.

[17] Robertson, J.; Powell, M. J. *Appl. Phys. Lett.* **1984**, *44*, 415–417.

[18] Robertson, J. *Philos. Mag., B* **1991**, *63*, 47–77.

[19] Robertson, J. *MRS Online Proceedings Library (OPL)* **1992**, *284*, 65.

[20] Robertson, J.; Warren, W.; Kanicki, J. *J. Non-Cryst. Solids* **1995**, *187*, 297–300.

[21] Warren, W. L.; Lenahan, P. M.; Curry, S. E. *Phys. Rev. Lett.* **1990**, *65*, 207–210.

[22] Krick, D. T.; Lenahan, P. M.; Kanicki, J. *Phys. Rev. B* **1988**, *38*, 8226–8229.

[23] Warren, W. L.; Lenahan, P. M. *Phys. Rev. B* **1990**, *42*, 1773–1780.

[24] Warren, W.; Kanicki, J.; Rong, F.; Poindexter, E. *J. Electrochem. Soc.* **1992**, *139*, 880.

[25] Warren, W.; Robertson, J.; Kanicki, J. *Appl. Phys. Lett.* **1993**, *63*, 2685–2687.

[26] Warren, W. L.; Kanicki, J.; Poindexter, E. H. *Colloids Surf. A: Physicochem. Eng. Asp.* **1996**, *115*, 311–317.

[27] Lenahan, P.; Krick, D.; Kanicki, J. *Appl. Surf. Sci.* **1989**, *39*, 392–405.

[28] Aiyama, T.; Fukunaga, T.; Niihara, K.; Hirai, T.; Suzuki, K. *J. Non-Cryst. Solids* **1979**, *33*, 131–139.

[29] Misawa, M.; Fukunaga, T.; Niihara, K.; Hirai, T.; Suzuki, K. *J. Non-Cryst. Solids* **1979**, *34*, 313–321.

[30] Wakita, K. W. K.; Hayashi, H. H. H.; Nakayama, Y. N. Y. *Jpn. J. Appl. Phys.* **1996**, *35*, 2557.

[31] Tsai, S.-J.; Wang, C.-L.; Lee, H.-C.; Lin, C.-Y.; Chen, J.-W.; Shiu, H.-W.; Chang, L.-Y.; Hsueh, H.-T.; Chen, H.-Y.; Tsai, J.-Y., et al. *Sci. Rep.* **2016**, *6*, 28326.

[32] Deshpande, S. V.; Gulari, E.; Brown, S. W.; Rand, S. C. *J. Appl. Phys.* **1995**, *77*, 6534–6541.

[33] Sahu, B. S.; Delachat, F.; Slaoui, A.; Carrada, M.; Ferblantier, G.; Muller, D. *Nanoscale Res. Lett.* **2011**, *6*, 1–10.

[34] Mohammed, S.; Nimmo, M. T.; Malko, A. V.; Hinkle, C. L. *J. Vac. Sci. Technol. A* **2014**, *32*, 021507.

[35] Ren, S.-Y.; Ching, W. *Phys. Rev. B* **1981**, *23*, 5454.

[36] Wu, C.-L.; Chen, W.-S.; Su, Y.-H. *Surf.Sci.* **2012**, *606*, L51–L54.

[37] Hintzsche, L.; Fang, C.; Watts, T.; Marsman, M.; Jordan, G.; Lamers, M.; Weeber, A.; Kresse, G. *Phys. Rev. B* **2012**, *86*, 235204.

[38] Hintzsche, L. E.; Fang, C. M.; Marsman, M.; Jordan, G.; Lamers, M. W. P. E.; Weeber, A. W.; Kresse, G. *Phys. Rev. B* **2013**, *88*, 155204.

[39] Kang, G.; Lee, D.; Lee, K.; Kim, J.; Han, S. *Phys. Rev. Appl.* **2018**, *10*, 064052.

[40] Wilhelmer, C.; Waldhoer, D.; Cvitkovich, L.; Milardovich, D.; Waltl, M.; Grasser, T. *Nanomaterials* **2023**, *13*, 2286.

[41] Marian, C. M.; Gastreich, M.; Gale, J. D. *Phys. Rev. B* **2000**, *62*, 3117–3124.

[42] Adabifiroozjaei, E.; Mofarah, S. S.; Ma, H.; Jiang, Y.; Assadi, M. H. N.; Suzuki, T. S. *Comput. Mater. Sci.* **2020**, *178*, 109632.

[43] Dasmahapatra, A.; Kroll, P. *Comput. Mater. Sci.* **2018**, *148*, 165–175.

[44] Chen, X.; Wang, Y.-W.; Liu, X.; Wang, X.-B.; Zhao, Y.-Q. *J. Non-Cryst. Solids* **2015**, *414*, 1–6.

[45] Pacchioni, G.; Erbetta, D. *Phys. Rev. B* **2000**, *61*, 15005.

[46] Di Valentin, C.; Palma, G.; Pacchioni, G. *J. Phys. Chem. C* **2011**, *115*, 561–569.

[47] Vianello, E. et al. In *2009 IEEE International Electron Devices Meeting (IEDM)*, IEEE: Baltimore, MD, USA, 2009.

[48] Milardovich, D.; Wilhelmer, C.; Waldhoer, D.; Cvitkovich, L.; Sivaraman, G.; Grasser, T. *J. Chem. Phys.* **2023**, *158*, 194802.

[49] Degraeve, R.; Cho, M.; Govoreanu, B.; Kaczer, B.; Zahid, M. B.; van den Bosch, G.; van Houdt, J.; Jurczak, M.; Groeseneken, G. In *2009 International Conference on Solid State Devices and Materials*, The Japan Society of Applied Physics: Sendai, 2009, pp 150–151.

[50] Gritsenko, V. A.; Perevalov, T. V.; Orlov, O. M.; Krasnikov, G. Y. *Appl. Phys. Lett.* **2016**, *109*, 062904.

[51] Gritsenko, V. A.; Kruchinin, V. N.; Prosvirin, I. P.; Novikov, Y. N.; Chin, A.; Volodin, V. A. *J. Exp. Theor. Phys.* **2019**, *129*, 924–934.

[52] Gritsenko, V. A.; Novikov, Y. N.; Shaposhnikov, A. V.; Morokov, Y. N. *Semiconductors* **2001**, *35*, 997–1005.

[53] Petersen, M.; Roizin, Y. *Appl. Phys. Lett.* **2006**, *89*, 053511.

[54] Mora-Fonz, D.; Shluger, A. L. *Adv. Electron. Mater.* **2020**, *6*, 1900760.

[55] Bersuker, G.; Sim, J.; Park, C.; Young, C.; Nadkarni, S.; Choi, R.; Lee, B. In *2006 IEEE International Reliability Physics Symposium Proceedings*, IEEE: San Jose, CA, USA, 2006, pp 179–183.

[56] Strand, J. W.; Cottom, J.; Larcher, L.; Shluger, A. L. *Phys. Rev. B* **2020**, *102*, 014106.

[57] El-Sayed, A.-M.; Watkins, M. B.; Afanas' ev, V. V.; Shluger, A. L. *Phys. Rev. B* **2014**, *89*, 125201.

[58] Waldhoer, D.; Schleich, C.; El-Sayed, A.-M.; Grasser, T. In *Oxide-based Materials and Devices XIV*, ed. by Teherani, F. H.; Rogers, D. J., SPIE: San Francisco, United States, 2023, p 10.

[59] Strand, J.; La Torraca, P.; Padovani, A.; Larcher, L.; Shluger, A. L. *J. Appl. Phys.* **2022**, *131*, 234501.

[60] Konstantinou, K.; Mocanu, F. C.; Lee, T.-H.; Elliott, S. R. *Nat. Commun.* **2019**, *10*, 3065.

[61] Konstantinou, K.; Elliott, S. R. *Phys. Status Solidi Rapid Res. Lett.* **2023**, *17*, 2200496.

[62] Gao, D. Z.; Strand, J.; Munde, M. S.; Shluger, A. L. *Front. Phys.* **2019**, *7*, 43.

[63] Anderson, P. W. *Phys. Rev.* **1958**, *109*, 1492.

[64] Bibyk, S. B.; Kapoor, V. J. *J. Appl. Phys.* **1981**, *52*, 7313–7316.

[65] Park, Y.; Jackson, W.; Johnson, N.; Hagstrom, S. *J. Appl. Phys.* **1990**, *68*, 5212–5221.

[66] Vedula, R. P.; Anderson, N. L.; Strachan, A. *Phys. Rev. B* **2012**, *85*, 205209.

[67] Kroll, P. *J. Non-Cryst. Solids* **2001**, *293-295*, 238–243.

[68] Toraya, H. *J. Appl. Crystallogr.* **2000**, *33*, 95–102.

[69] Schmidt, J.; Schuurmans, F. M.; Sinke, W. C.; Glunz, S. W.; Aberle, A. G. *Appl. Phys. Lett.* **1997**, *71*, 252–254.

[70] Gritsenko, V. A.; Nekrashevich, S. S.; Vasilev, V. V.; Shaposhnikov, A. V. *Microelectron. Eng.* **2009**, *86*, 1866–1869.

[71] Midya, K.; Dhar, S.; Kottantharayil, A. *J. Appl. Phys.* **2013**, *114*, 154101.

[72] Novikov, Y. N.; Gritsenko, V. A. *J. Non-Cryst. Solids* **2020**, *544*, 120186.

[73] Kim, T. H.; Park, I. H.; Lee, J. D.; Shin, H. C.; Park, B.-G. *Appl. Phys. Lett.* **2006**, *89*, 063508.

[74] Sanjoh, A.; Ikeda, N.; Komaki, K.; Shintani, A. *J. Electrochem. Soc.* **1990**, *137*, 2974.

[75] Solanki, R.; Manwani, A.; Mahajan, A.; Patrikar, R. M. *Superlattices and Microstruct.* **2020**, *144*, 106577.

[76] Sung, J.-Y.; Jeong, J.-k.; Nam, K.-R.; Lee, G.-W. *Trans. Electr. Electron. Mater.* **2021**, *22*, 432–438.

[77] Thompson, A. P.; Aktulga, H. M.; Berger, R.; Bolintineanu, D. S.; Brown, W. M.; Crozier, P. S.; in 't Veld, P. J.; Kohlmeyer, A.; Moore, S. G.; Nguyen, T. D.; Shan, R.; Stevens, M. J.; Tranchida, J.; Trott, C.; Plimpton, S. J. *Comput. Phys. Commun.* **2022**, *271*, 108171.

[78] Le, V. V.; Dinh, T. H. *J. Non-Cryst. Solids* **2022**, *581*, 121381.

[79] Nosé, S. *J. Chem. Phys.* **1984**, *81*, 511–519.

[80] Nosé, S. *Mol. Phys.* **1984**, *52*, 255–268.

[81] Hoover, W. G. *Phys. Rev. A* **1985**, *31*, 1695–1697.

[82] Le Roux, S.; Jund, P. *Comput. Mater. Sci.* **2010**, *49*, 70–83.

[83] Goetzke, K.; Klein, H.-J. *J. Non-Cryst. Solids* **1991**, *127*, 215–220.

[84] Yuan, X.; Cormack, A. N. *Comput. Mater. Sci.* **2002**, *24*, 343–360.

[85] Kühne, T. D. et al. *J. Chem. Phys.* **2020**, *152*, 194103.

[86] VandeVondele, J.; Hutter, J. *J. Chem. Phys.* **2007**, *127*, 114105.

[87] Goedecker, S.; Teter, M.; Hutter, J. *Phys. Rev. B* **1996**, *54*, 1703–1710.

[88] Hartwigsen, C.; Goedecker, S.; Hutter, J. *Phys. Rev. B* **1998**, *58*, 3641–3662.

[89] Perdew, J. P.; Burke, K.; Ernzerhof, M. *Phys. Rev. Lett.* **1996**, *77*, 3865–3868.

[90] Perdew, J. P.; Burke, K.; Ernzerhof, M. *Phys. Rev. Lett.* **1997**, *78*, 1396.

[91] Heyd, J.; Scuseria, G. E.; Ernzerhof, M. *J. Chem. Phys.* **2003**, *118*, 8207–8215.

[92] Heyd, J.; Scuseria, G. E.; Ernzerhof, M. *J. Chem. Phys.* **2006**, *124*, 219906.

[93] Guidon, M.; Hutter, J.; VandeVondele, J. *J. Chem. Theor. and Comp.* **2010**, *6*, 2348–2364.

[94] Lany, S.; Zunger, A. *Model. Simul. Mat. Sci. Eng.* **2009**, *17*, 084002.

[95] Komsa, H.-P.; Rantala, T. T.; Pasquarello, A. *Phys. Rev. B* **2012**, *86*, 045112.

[96] Bell, R. J.; Dean, P. *Discuss. Faraday Soc.* **1970**, *50*, 55–61.

[97] Dong, J.; Drabold, D. A. *Phys. Rev. B* **1996**, *54*, 10284–10287.

[98] Unge, M.; Christen, T. *Chem. Phys. Lett.* **2014**, *613*, 15–18.

[99] Youn, Y.; Kang, Y.; Han, S. *Comp. Mat. Sci.* **2014**, *95*, 256–262.

[100] Chang, T.-M.; Bauer, J. D.; Skinner, J. L. *J. of Chem. Phys.* **1990**, *93*, 8973–8982.

[101] Humphrey, W.; Dalke, A.; Schulten, K. *J. Mol. Graph.* **1996**, *14*, 33–38.